BNL-65905

ATMOSPHERIC OPTICAL PROPERTIES OVER THE RUSSIAN STEPPE DURING SUMMER

R. N. Halthore, V. V. Kozoderov, E. I. Nezval, N. E. Chubarova,
L.A. Shljakhova, and B. Markham

Environmental Chemistry Division
Department of Applied Science
Brookhaven National Laboratory
Upton, NY 11973-5000

October 1998

Published in
Remote Sensing Reviews
[17, 221-238, 1998]

By acceptance of this article, the publisher and/or recipient acknowledges the U.S. Government's right to retain a non exclusive, royalty-free license in and to any copyright covering this paper.

Research by BNL investigators was performed under the auspices of the U.S. Department of Energy under Contract No. DE-AC02-98CH10886.

Remote Sensing Reviews, Vol. 12, pp. 221–238
Reprints available directly from the publisher
Photocopying permitted by license only

© 1995 OPA (Overseas Publishers Association) N.V.
Published by license under
the Harwood Academic Publishers imprint,
part of The Gordon and Breach Publishing Group.
Printed in India.

Atmospheric Optical Properties over the Russian Steppe during Summer

RANGASAYI N. HALTHORE[a,*], VLADIMIR V. KOZODEROV[b], ELEANA I. NEZVAL[c], NATALIA E. CHUBAROVA[c], LUDMILA A. SHLJAKHOVA[d] and BRIAN L. MARKHAM[e]

[a]*Department of Applied Science, Brookhaven National Laboratory, Upton, NY 11973-5000, USA;* [b]*Institute of Computational Mathematics, Russian Academy of Sciences, Leninsky Prospect, 32A, Moscow, Russia 117334;* [c]*Meteorological Observatory of Moscow State University, Leninskiye Gory, Moscow, Russia 119899;* [d]*Regional Donecocenter, Prospect Sokolova, 52, Rostov-on-Don, Russia 344700;* [e]*Biospheric Sciences Branch, NASA Goddard Space Flight Center, Greenbelt, MD 20771, USA*

Atmospheric transmittance is estimated by measuring the direct-normal solar irradiance at the surface by a sun-photometer or a spectro-radiometer. Both of these types of instruments were used to determine the most variable components of the atmospheric transmission, aerosol optical thickness (AOT) and precipitable water vapor (PW) in cm, during an international field experiment, KUREX'91, held in July, 1991 in the Streletskaya Steppe Biospheric Reserve near Kursk, Russia. A narrow field of view sun-photometer provided AOT in 7 discrete spectral channels from 440-nm to 1030-nm and PW from observations in the 940-nm channel. A spectro-radiometer provided AOT at 70 spectral intervals in the 380-nm to 550-nm range. The latter also provided measurements of diffuse sky irradiance at the surface. Both the instruments were calibrated by the Langley plot method or the long-Bouguer method as it is known in the Russian literature. The derived AOT are inverted to obtain aerosol size distribution with the help of an algorithm based on Twitty's method. Size distributions derived by extinction measurements are compared with those derived from aureole measurements. Results from KUREX'91 show that on some days a significant portion of aerosols may be mono-disperse, indicating their anthropogenic origin.

Keywords. Aerosol optical thickness; Sun-photometers; Aerosol size distribution; Precipitable water; Spectro-radiometer

* Corresponding author.

INTRODUCTION

Water vapor and aerosols contribute major uncertainties in estimation of the components of the global radiation budget. Accurate estimates of water vapor abundance are necessary to correctly predict the extent of atmospheric absorption of solar energy and the resulting atmospheric emission to space. Accurate estimates of aerosol optical properties including aerosol optical thickness, single scattering albedo (a measure of scattering to extinction ratio) and asymmetry parameter (a measure of angular distribution of scattered light) are required to predict the effect of aerosols on the net radiation budget. The latter effect could be negative, meaning that the effect of aerosols could be a net cooling of the atmosphere counteracting the greenhouse warming due to increase in absorbing gases. Of immediate concern to many of the international groups of scientists gathered in July, 1991 at the Streletskaya Steppe Biospheric Reserve near Kursk in the southern part of Russia, was the possibility of accurate estimates of surface biophysical properties by remote sensing. Relationship of surface parameters such as reflectance and temperature (and their derived parameters such as the vegetation biomass, leaf area index and photosynthetically active radiation) to the at-sensor radiance is obtained using models that describe the radiation field in the earth–atmosphere system with varying degrees of complexity and accuracy. The models typically perform *atmospheric correction* – a term that denotes the fact that in surface studies atmospheric interaction with the radiance field is noise that should be eliminated.

Estimate of the surface or atmospheric properties from remotely sensed data requires the knowledge of components of the atmosphere that have the maximum effect on the out-going radiation (as sampled by a satellite or an aircraft). Atmospheric correction of remotely sensed data is now accepted as an integral part of any research that requires retrieval of surface properties from sensors aboard satellite and aircraft platforms. Halthore and Markham (1992) showed that uncertainty in the measurement of AOT and PW have comparable effect on the retrieval of surface reflectance in those bands that do not include the major water absorption bands. An uncertainty in AOT of 0.01, routinely achieved at present by performing calibration at mountain sites before and after a field experiment directly translates to a 1% accuracy in the retrieved surface reflectance. Except under fairly turbid atmospheric conditions, measurement uncertainties in atmospheric transmission are one of the most important quantities that affect the retrieval of surface properties from remote data;

under turbid atmospheric conditions, insufficient accuracy in the multiple scattering algorithms are more important than the AOT uncertainty.

In this paper, we report measurements of total and aerosol optical thickness, and water vapor column abundance during a period of 3 weeks beginning July 6, 1991 and ending on July 25, 1991. We also report aerosol size distribution obtained by inversion of AOT versus wavelength curves and validate the distribution by comparison with a method that obtains size distribution by inverting the solar aureole radiance.

INSTRUMENTS

Results from an eight channel, auto-sun tracking sunphotometer, commonly known as SXM-2 (Halthore et al., 1990, 1992b), built at the NASA Goddard Space Flight Center, Greenbelt, Maryland, USA, are presented here. Data were acquired and stored automatically on a computer. Of the eight channels at 441, 522, 613, 672, 781, 872, 940 and 1030 nm, the 940 nm channel is coincident with the strong water vapor absorption band and is thus used to derive water column abundance (Halthore et al., 1997); the other 7 channels provide the vertical aerosol optical thickness (AOT). The bandwidth of aerosol channels was between about 10 and 20 nm (full width at half maximum, FWHM) whereas that of the 940 nm channel was 40 nm. The SXM-2 has a 1.2° field-of-view and can be operated in the sky scanning mode although only data from the sun-tracking mode are analyzed here. The instrument cycles through all the channels in about 10–15 s with a minimum repetition rate of 30 s employed during periods of rapid airmass change in the mornings and evenings. The maximum delay between cycles, 4 min, was employed during afternoons when the change in airmass is relatively small.

The spectro-radiometer built at the Meteorological Observatory of the Moscow State University (hereafter MSU), Moscow, Russia, measures direct, diffuse and total solar irradiance in the range 300–580 nm with a nominal spectral resolution of 2 nm at 300 nm and 10 nm at 575 nm. Irradiance is measured in 70 narrow spectral bands, 44 of them being in the UV range. It consists of a double-monochromator with quartz optics (Vysotsky et al., 1982) with an "integrating checker" placed at the entrance slit. The integrating checker allows a view angle of 180° and consists of a metal hemisphere surrounded by a hemispheric quartz cap with a screen and tube containing diaphragms which exclude direct solar radiation from falling on the slit. This type of checker possesses a greater

light gathering power than the usual photometric spheres. Collimators (tubes) are changed to observe the sun with a 5° field of view for direct irradiance or exclude 10° around the sun for a diffuse sky measurement. Thus, the direct solar irradiance measurement is accomplished much as in a sun-photometer with the use of a narrow angle collimator. Sensitivity control of the instrument during field measurements is obtained by checking against an incandescent lamp at 534 nm.

METHOD

Application of Bouguer's law (also known as Bouguer–Lambert–Beer (B-L-B) law) forms the basis of atmospheric optical thickness measurement in channels that do not include molecular band absorption (i.e., 940 nm band). The theoretical basis is extensively discussed in literature (Shaw, 1983) and is relatively simple and straightforward. It follows from the Bouguer's basic assumption that the attenuation of a beam of irradiance is linearly proportional to the amount of matter in the intervening path. For those channels that include a molecular absorption band, the attenuation with distance is not necessarily linearly proportional to the amount of matter. There are three types of light attenuation – molecular scattering or Rayleigh scattering, aerosol attenuation by scattering and absorption, and trace gas absorption. In Rayleigh scattering molecules which have dimensions much smaller than the wavelength of light, attenuate light by dipole interaction that is strongly dependent on the frequency of light. In fact, Rayleigh showed that the scattering cross-section is proportional to 4th power of the frequency; thus blue light in the sky is attenuated much more strongly than the red. Particles or aerosols having dimensions comparable to the wavelength of light interact strongly with the light in a complex way; the theory for spherical particles was developed by Mie and this type of interaction is therefore known as Mie scattering. Trace gases such as ozone, carbon-dioxide and water that possess a permanent dipole moment absorb incoming energy into many of their internal energy modes such as vibration, rotation and electronic manifolds in specific transitions of their internal energy states giving the appearance of "line" spectra in any of their molecular absorption bands. Since absorption occurs according to Bouguer's law within those lines, light energy in the original beam is preferentially attenuated within those lines and subsequent passage of light through matter proceeds with little attenuation outside of those lines but within the band. This is the origin

of non-linear dependence of attenuation on column abundance. Continuum absorption by ozone and water vapor still follows Bouguer's law, however.

If V is the voltage response of the sun-photometer to solar irradiance at the ground,

$$V = (V_0/r^2)\exp((-m\tau)_R - (m\tau)_{oz} - (m\tau)_{aer})T_W, \tag{1}$$

where V_0 is the calibration coefficient and represents the fictitious instrument response to exo-atmospheric solar irradiance when the Earth–Sun distance r is 1 Astronomical Unit (AU) (the mean distance). The airmass m depends in general on the attenuator denoted by subscript R for Rayleigh scattering, oz for ozone continuum absorption and aer for aerosol scattering and absorption. These components are assumed to follow Bouguer's law of attenuation where the optical thickness is linearly dependent on column abundance. For the channel containing the water absorption band (940 nm band), the water absorption does not follow Bouguer's law and instead the transmission T_W is written as (Halthore et al., 1992a; Bruegge et al., 1992),

$$T_W = \exp(-aw^b) = \exp(-aW^b m^b), \tag{2}$$

where w is the path water abundance in $\mathrm{g\,cm^{-2}}$, W is the precipitable water (vertical column abundance) in $\mathrm{g\,cm^{-2}}$ or cm of water, and a and b are constants to be determined independently by the use of a radiative transfer algorithm. The procedure to obtain coefficients a and b is described in Halthore et al. (1997); MODTRAN (Version 1.1) was used in conjunction with "standard atmospheres" to analyze Kursk data. Substituting Eq. (2) in Eq. (1) and rearranging, we have

$$\ln(V) + (m\tau)_R + (m\tau)_{oz} + (m\tau)_{aer} = \ln(V_0/r^2) - aW^b m^b. \tag{3}$$

A plot of the left-hand side of this equation versus m^b is linear if W does not change during the period of measurement and the y intercept then gives the calibration coefficient V_0. The aerosol optical thickness in the water band for estimating the left hand side of Eq. (3) is obtained by an Ångström interpolation (that is, using $\tau \sim \alpha\lambda^{-\beta}$, where α and β are Ångström coefficients). Equation (3) forms the basis of water vapor column abundance measurement using sun-photometers or enables measurement of AOT in non-water absorbing channels by neglecting the last term on the right-hand side. Rayleigh optical thickness is accurately

determined by a measurement or estimate of surface pressure and ozone contribution is estimated from known absorption cross-sections and abundance estimates from climatology. Determination of V_0 in Eq. (3) requires calibration for sun-photometers and is discussed next.

CALIBRATION

For non-water absorbing channels, a plot of $[\ln(V) + (m\tau)_R + (m\tau)_{oz}]$ versus m_{aer} produces a straight line with $[\ln(V_0/r^2)]$ as the y-intercept for zero airmass, provided AOT remains constant during calibration. This is the well known Langley plot or the long-Bouguer method. Likewise, a plot of left-hand side of Eq. (3) versus m^b allows the calibration coefficient V_0 to be determined provided both AOT and W remain constant during calibration. This is generally termed as the Modified Langley Method (MLM) after Reagan et al. (1987). Conditions most favorable for calibration are at mountain sites well above the local boundary layer during mornings when the airmass change is maximum and during which time the convective currents from below have not had a chance to affect the measurements.

Calibration of SXM-2 was made at two sites: one before KUREX'91 in June, 1991 at Sunspot (2805 m elevation) in New Mexico; and the other after KUREX'91 in September, 1991 at Mauna Loa (elevation: 3963.4 m) in Hawaii. By September the effects of Pinatubo volcano (on the island of Luzon, Philippines), which erupted on June 15, caused an increase in the stratospheric aerosol optical thickness at Mauna Loa to unacceptable levels for calibration. Measured AOT values on September 28 on Mauna Loa were 0.21, 0.17, 0.166, 0.161, 0.15, and 0.14 at 441, 522, 613, 672, 781 and 872 nm, respectively. Note that background AOT values are typically of the order of 10^{-3} at Mauna Loa. Thus post-KUREX'91 calibration for the AOT channels could not be achieved. For the water channel, due to the large band width, the signal saturated at low airmass at both the mountain sites so that calibration was performed only at high airmass. Calibration in Hawaii yielded good results for the water channel owing to the low column abundance of water vapor; presence of stratospheric aerosols from the Pinatubo eruption had no effect. At Sunspot in New Mexico, pre-KUREX'91 calibration yielded V_0's from three good Langley plots in most channels which differed from each other by less than 1%. The aerosol optical thickness was relatively low approximately in the range 10^{-2}–10^{-1} in the visible channels. Inter-comparison with a hand

held sun-photometer before and during KUREX'91 showed that neither instrument had degraded and that the calibration coefficients obtained at Sunspot were reliable. We estimate that the accuracy in the calibration to be in the 1–2% range.

For the calibration of the 940 nm channel using the MLM method, we use MODTRAN (Version 1.1) and the mid-latitude summer atmospheric profile available in the program itself to determine a and b in Eq. (2). Specifically, we ran MODTRAN in the transmission mode and then convolved the resulting transmittance with the 940 nm channel filter function to obtain the band transmission. The transmittance T_W is calculated at various solar zenith angles for known path water abundance w. A plot of $\log(\log(1/T_W))$ versus $\log(w)$ gives a straight line whose slope is b and whose y-intercept is $\log(a)$. Halthore et al. (1997) have shown that for a broad band 940 nm channel, such as that used here, coefficients a and b are sensitive functions of the type of atmosphere used during calibration and during measurement. Ideally radiosonde data should be used during both calibration and measurement. As the radiosonde data were unavailable during this campaign we used standard atmospheres from climatology for much of the data analysis; therefore we expect the derived water column abundance to have a large uncertainty, perhaps in the 10–15% range.

Absolute calibration of the direct-normal solar irradiance as measured by the MSU spectro-photometer was made using the long-Bouguer's (Langley) method. Furthermore, the spectral resolution of the instrument was characterized taking into account monochromator aperture functions, dispersion of prisms, rate of running the spectra, and time of averaging initial signals. Exo-atmospheric solar radiation as a function of wavelength was applied in accordance with the World Meteorological Organization recommendations to calibrate instrument response for the direct, diffuse and total downward irradiance. The spectral resolution was found to vary from 1.9 nm at 297 nm to 9.6 nm at 575 nm. The cosine correction was less than 10% for solar zenith angle less than 70° and was within 1–3% when the solar zenith angle was less than 60°. For the analysis of the MSU data, the total ozone content was assumed constant for the entire field campaign and equal to average values for Voronezh (0.36 atm-cm or 360 Dobson Units (DU), July 1991), a town that is near Kursk and the nearest station belonging to the ozonometric network. The variability for July 1991 was ± 0.025 atm-cm and this leads to an uncertainty in the AOT of about 12% in visible spectral bands. Halthore and Markham (1992) calculated that at the peak of the Chappuis band ($\sim 0.6\,\mu$m) the

ozone optical thickness due to 300 DU of ozone is 0.04; thus for an uncertainty of 25 DU in ozone column abundance, this translates to an uncertainty in AOT of 0.003.

RESULTS AND DISCUSSION

Measurements with the SXM-2 were possible on July 7 (900–1500 hours, local clock time), 8 (900–1500), 9 (900–1100), 14 (800–1400), 17 (830–1500), 20 (900–1850), 21 (600–1000), 22 (1245–1330) and 25 (830–1130). Other days and times were either clouded out and rained out except for July 10 which was a clear day but had been predetermined to be a rest day. The Kursk local clock time is 3 h ahead of UT. Aerosol optical thickness values (Fig. 1) varied from a low of 0.02 on July 14 to a

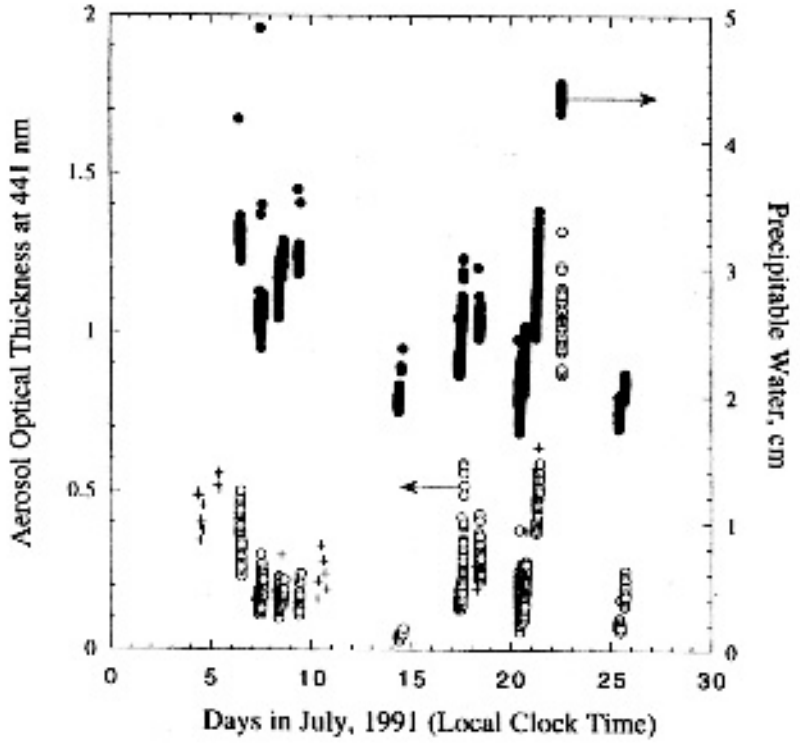

FIGURE 1 AOT (open circle) at 441 nm and PW (cm) (filled circle) are plotted for the whole KUREX'91 campaign from July 6 to July 25, 1991. Abscissa refers to time in days in July – 12.00 noon local clock time on July 6 is plotted as 6.5. Also shown are AOT at 439 nm (+) as measured by MSU. The local clock time is 3 h ahead of UT.

high of 1.3 on July 22 for the 441 nm channel. The range for the precipitable water was 1.7 (July 14) to 4.3 (July 22). Table I gives the averaged values of the aerosol optical thickness in three channels (441, 672, 872 nm) and the precipitable water in cm for the duration of KUREX'91. Within each time period, the values may change considerably as can be seen from Fig. 1. In an earlier report on the KUREX'91 measurements (Halthore et al., 1992a), we had presented a version of Table I with PW values that were derived using LOWTRAN-7, a low resolution radiative transfer model. The current values based on MODTRAN are seen to be about 9% higher and do not have the problem of misinterpretation of LOWTRAN7 results. AOT and PW values on July 14 are among the lowest and can be explained by the presence of cold, dry, clean Arctic airmass brought in by the passage of a cold front on July 12. The highest values of AOT and PW seen on July 22 are the result of an apparently easterly flow of 7 m/s in the boundary layer (A. Grin, private communication, 1991) that brought in the airmass from south-eastern part of European Russia. AOT as measured by the MSU is also plotted in Fig. 1; the values are usually well within ± 0.05 of those of SXM-2 showing that the independently calibrated instruments give consistent results. Also apparent in Fig. 1 and Table I is the correlation between AOT and PW. Correlation coefficient among the AOT values in different channels is better than 0.97 (R^2) and that between any of the AOT channels and

TABLE 1 Average values of AOT and PW measured by SXM-2 for some select intervals

Date	*Kursk clock time*	*Aerosol optical thickness*			*Precipitable water*, cm
		441 nm	673 nm	872 nm	
7/7	900–1200	0.14	0.07	0.06	2.60
7/8	1100–1200	0.16	0.08	0.06	3.00
	1300–1400	0.15	0.09	0.07	3.00
7/9	915–945	0.12	0.08	0.06	3.00
7/14	830–1000	0.04	0.02	0.02	1.97
	1000–1200	0.03	0.02	0.01	2.15
	1200–1400	0.05	0.04	0.03	2.26
7/17	830–1300	0.15	0.07	0.05	2.30
	1300–1400	0.2	0.1	0.06	2.62
7/20	900–1000	0.18	0.1	0.06	1.97
	1000–1200	0.11	0.06	0.04	1.86
	1200–1300	0.22	0.12	0.08	2.18
	1300–1400	0.25–0.1	0.12–0.08	0.08–0.06	2.18
	1400–1600	0.13	0.09	0.06	2.18
	1600–1800	0.17	0.1	0.07	2.40
7/21	700–800	0.43	0.22	0.14	3.05
7/22	1300	0.9	0.55	0.35	4.53
7/25	830–1130	0.07	0.04	0.03	1.80

PW is about 0.75. In the First International Satellite Land Surface Climatology Project (ISLSCP) Field Experiment (FIFE) held in 1987 and 1989 on surface terrain and location similar to the one at Kursk, the correlation coefficient between AOT (440 nm) and specific humidity was found to be 0.8 and 0.1 respectively (Halthore et al., 1992b). Thus the current finding is more similar to FIFE'87 than FIFE'89 in this regard.

Spectral features of the total and aerosol optical thicknesses (TOT and AOT) as measured by MSU are shown in Fig. 2. Not surprisingly the total optical thickness is increasing with decrease in wavelength at a much faster rate than the AOT because of increased Rayleigh scattering. The role of aerosols increases with wavelength in the visible region. For example, for the clear day 7/7/91, the ratio of AOT/TOT has increased

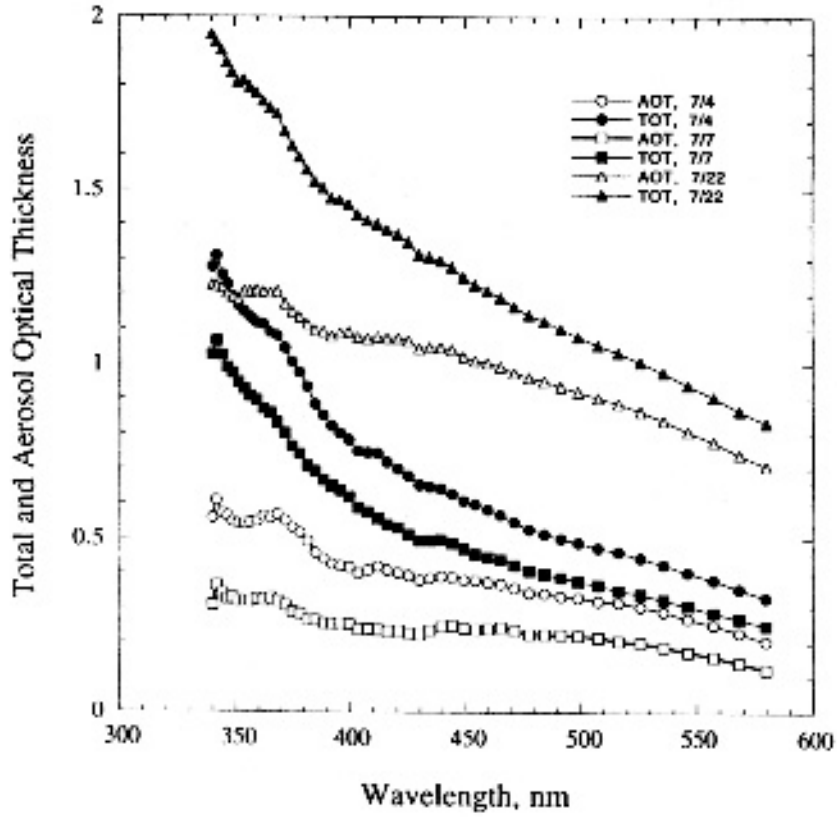

FIGURE 2 MSU measured AOT (open symbols) and Total optical thickness (TOT) (filled symbols) are plotted as a function of wavelength for three days – 7/7/91 (low turbidity, squares), 7/4/91 (medium, circles); and 7/22/91 (high, triangles). The number and location of symbols on 7/4/91 depict the number of spectral channels on the MSU.

from 0.33 at 340 nm to 0.50 at 580 nm. For the day of high opacity (7/22/91) the aerosol fractional contribution increases from 0.62 to 0.83 at the same wavelengths. For all days, the difference between TOT and AOT is constant at any given wavelength because a constant ozone column abundance was used to derive AOT; because of ozone absorption, this difference does not follow the $(1/\lambda^4)$ dependence.

The ratio of total hemispherical downward irradiance at the surface to extra-terrestrial downward irradiance is a measure of the atmospheric transmission. For zero surface reflectance, the ratio is in fact the vertical transmittance of the atmosphere. This ratio, which is the normalized surface irradiance, is plotted in Fig. 3 for three solar zenith angles on

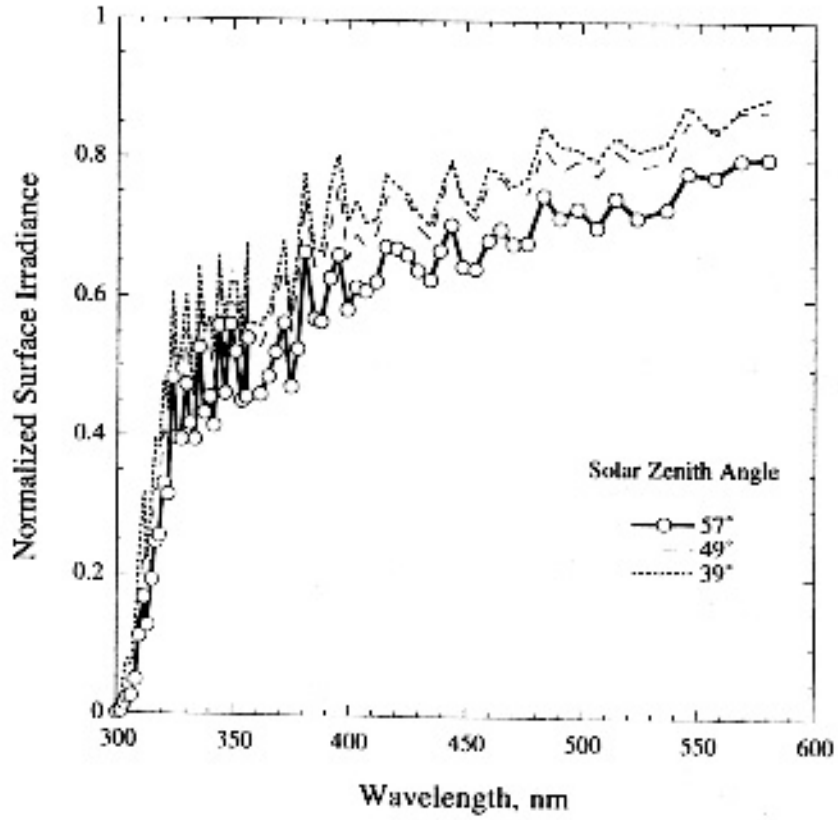

FIGURE 3 Normalized surface irradiance, the ratio of total hemispherical downward irradiance and extra-terrestrial downward solar irradiance at 1 AU is plotted for three solar zenith angles – 57 (solid line with open circles), 49 (long dashed line) and 39 (short dashed line) on July 20, 1991. The ordinate is a measure of the total transmittance; ozone absorption below 320 nm dominates this spectrum.

July 20 from MSU measurements of the total surface irradiance. The extra-terrestrial value refers to the mean Earth–Sun distance of 1 AU. Increasing solar zenith angle decreases the ratio as expected. The transmittance depends strongly on the wavelength with the sharp drop for wavelengths shortward of 330 nm caused by ozone absorption.

Ångström exponent is an indicator of the type of airmass present during measurements. It is the slope of the log(AOT) versus log(wavelength) curve. In general high values of the exponent indicate the presence of clean continental airmass containing small particles, and values close to zero (flat curves) are caused by the presence of large particles such as those found in desert environments or humid, urban environments. Cirrus clouds typically have values less than 0.5. Figure 4 shows a histogram of

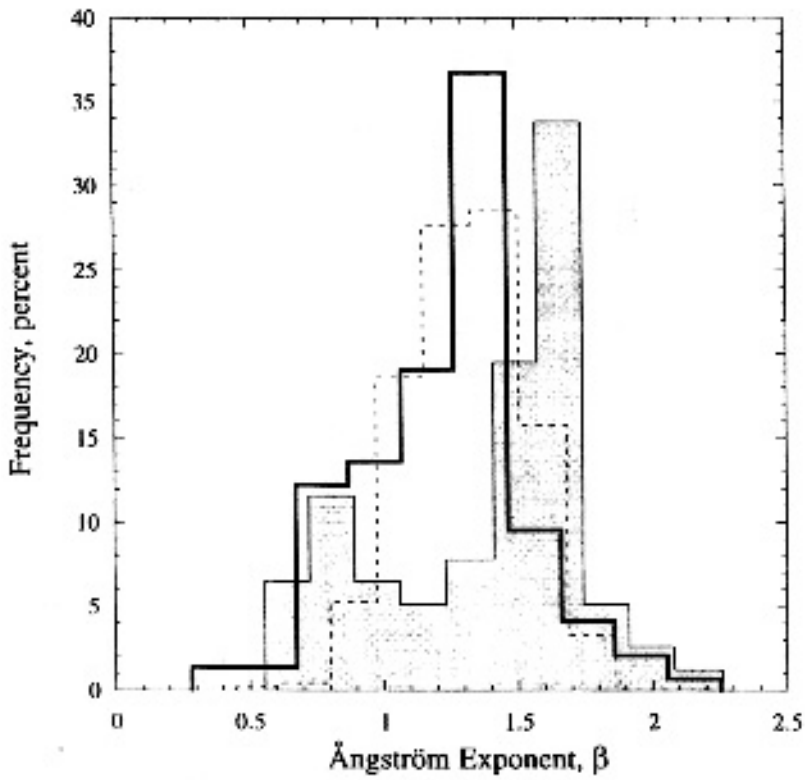

FIGURE 4 Histogram of Ångström exponents for 1,460 measurements in KUREX'91 (solid line) is plotted and compared with those obtained in FIFE'87 (77 measurements, shaded) and in FIFE'89 (147 measurements, dashed line). Bi-modal distribution seen in FIFE'87 is not seen in KUREX'91 or in FIFE'89. Mean and standard deviation are 1.311 ± 0.214, 1.39 ± 0.385, 1.22 ± 0.305 for KUREX'91, FIFE'87 and FIFE'89 respectively.

the Ångström exponent for all the data obtained by SXM-2 in KUREX'91. Over 80% of the Ångström plots had a goodness of least square fit (R^2) close to 0.97 (see Fig. 6(a)). However, there were many cases, significantly on July 14 when the AOT was lowest and on July 25, that the R^2 was below 0.9. There were episodes on other days as well with R^2 below 0.9. We will argue with the aid of inferred size distribution that such a deviation from Ångström fit may be the result of the presence of mono-disperse aerosols, primarily man-made, rather than a broader, power-law type distribution characteristic of natural aerosols.

Superimposed on the histogram in Fig. 4 are also the results of FIFE'87 and FIFE'89 field campaigns. The bimodal distribution observed in 1987 is not seen in the other two curves. In FIFE'87 the presence of two contrasting airmasses – one cool, clean and dry continental airmass and the other wet, turbid and warm "gulf" airmass (meaning that the origin of this airmass was in the Gulf of Mexico) – undoubtedly caused this bimodal distribution. The gulf airmass had values less than 1, whereas the continental airmass had values greater than 1. No such clear distinction was possible in 1989 or here in KUREX'91 data. We observe that the mean value of the Ångström exponent is close to 1.31, less than 1.6 observed for the continental airmass in FIFE'87, so that a indistinguishable mixture of continental and marine airmass may have been present during this experiment. Detailed measurements of the aerosol single scattering albedo, composition and phase function or accurate trajectory analysis are not available to present definitive arguments.

We further explore the behavior of Ångström exponent in this field experiment with the aid of aerosol size distribution inversions. Here we use the method of Twitty (1974) wherein the expression for AOT (τ) as a function of wavelength λ,

$$\tau(\lambda) = \int Q_{\text{ext}}(r, \lambda, \mu)\pi r^2 \left(\frac{\mathrm{d}N}{\mathrm{d}r}\right)\mathrm{d}r,$$

is inverted to obtain the column averaged size distribution ($\mathrm{d}N/\mathrm{d}r$) in units of $\#\,\mu\mathrm{m}^{-2}\,\mu\mathrm{m}^{-1}$. Extinction efficiency Q_{ext} is computed by a Mie scattering code (Dave, 1968) as a function of size parameter (defined as $2\pi r/\lambda$, where r is the radius of the particle) and refractive index μ. The latter is assumed in the absence of measurements of the aerosol composition to be $1.41 \pm 0.00001\mathrm{i}$, a value that is considered typical of aerosols at mid-latitudes. The inversion was first tested for the case of perfect Ångström behavior ($\tau \sim a\lambda^{-b}$) to obtain a size distribution ($\mathrm{d}N/\mathrm{d}r \sim cr^{-1}$)

with $r = b + 3$. Next we tested the code against an independent and complementary method that inverts the solar aureole measurements of a sky-scanning sun-photometer to yield size distribution (Nakajima et al., 1983). Figure 5 shows the result of inverting by the two methods for the AOT and the aureole radiance data taken by the same instrument (in this case a Cimel sun-photometer) at almost the same time. The two methods are complementary since while the AOT is indicative of the extinction efficiency, the solar aureole brightness depends on the scattering efficiency for scattering in the predominantly forward direction. Forward scattering is sensitive to large particles due to the large asymmetry factor (close to 1). The comparison in Fig. 5 is for data taken at Department of Energy's

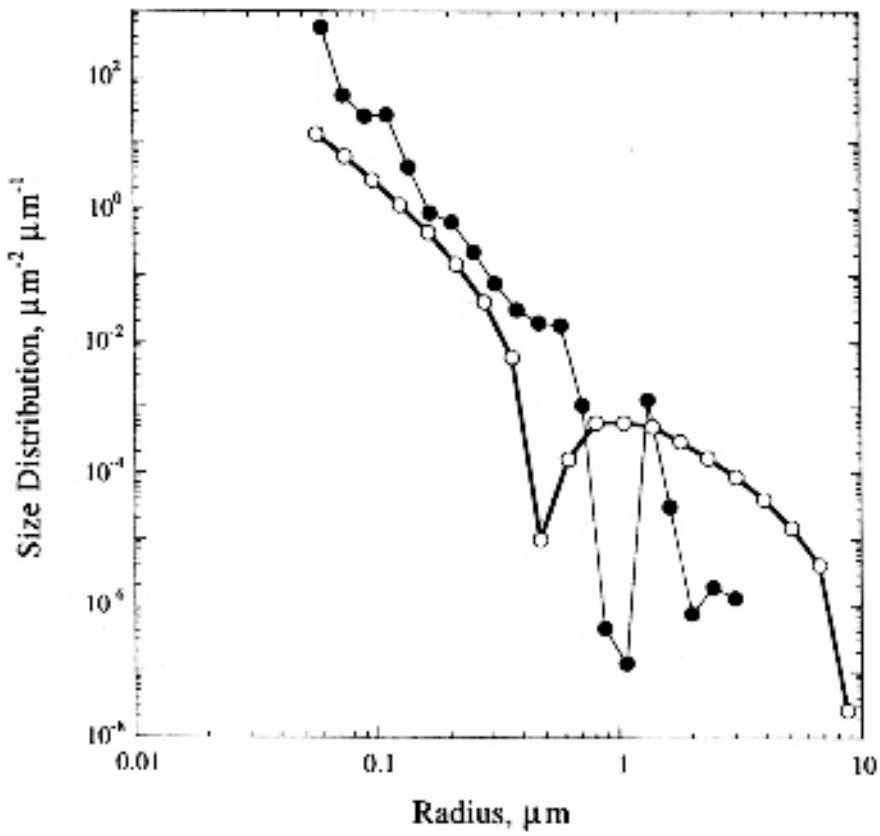

FIGURE 5 Columnar size distribution as derived by Nakajima's method (open circles) from the solar aureole radiance is compared with that derived by Twitty's method (filled circles) from the AOT versus wavelength curve. Data are obtained at the CART ARM site in North-Central Oklahoma on September 27, 1997.

Atmospheric Radiation Measurement Site at Lamont, Oklahoma on September 27, 1997, which was a clear day, devoid of clouds. The radius interval was restricted in Twitty's method to 0.06–3 μm since particles outside this size range do not uniquely interact with sunlight in the extinction mode. Even then, the comparison shown in Fig. 5 depicts what could be construed as oscillations due to insensitivity of the numerical procedure to invert the above equation. Nevertheless the comparison between the two methods yields consistent results with the Twitty's method yielding more smaller size particles than Nakajima's method.

Three Ångström plots representing three days of varying turbidity are shown in Fig. 6(a). The Ångström fit is seen to be good ($R^2 > 0.99$) for the two high (7/22) and medium (7/6) turbidity days while it is not as

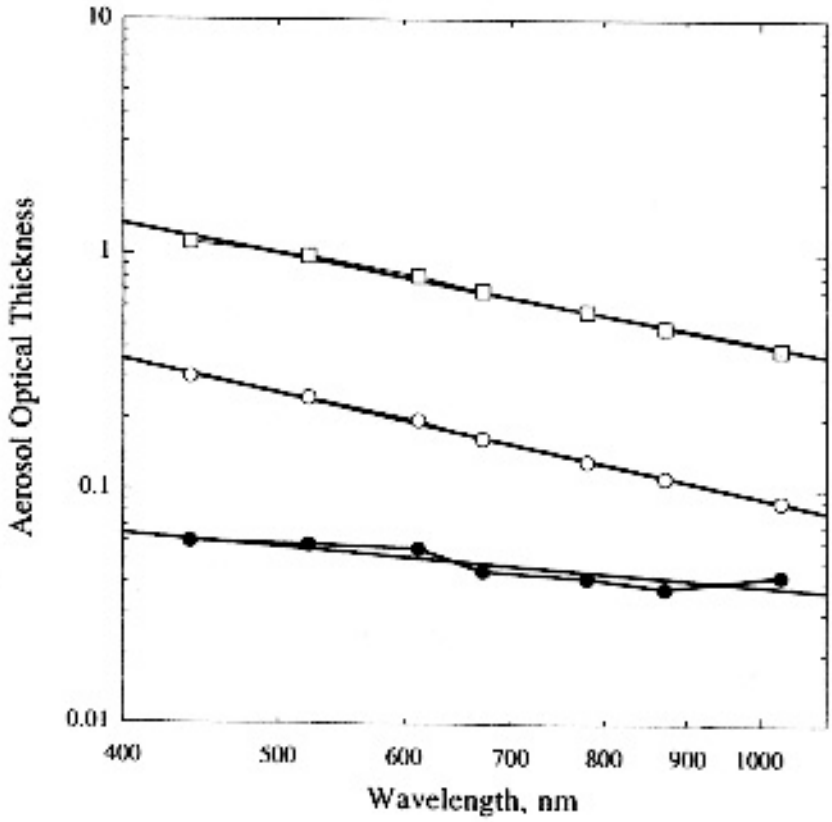

FIGURE 6(a) Ångström plots are shown for three instances on three contrasting days: low turbidity (7/14, filled circles); moderate turbidity (7/6, open circles) and high turbidity (7/22, squares). Least-squares fits to the data shown here, yield the Ångström exponent.

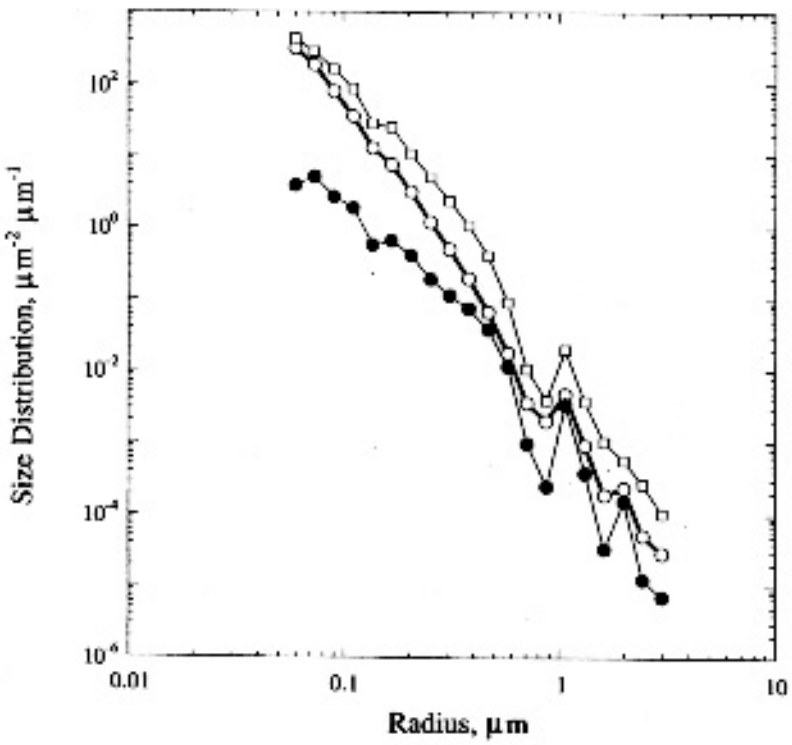

FIGURE 6(b) Number size distribution derived by Twitty's method is compared for three contrasting days shown in Fig. 6(a). Same symbols as in Fig. 6(a) are used here.

good (< 0.9) for the low (7/14) turbidity day. The size distribution shown in Fig. 6(b) confirms the fact that indeed there are a lot more particles of all sizes but especially smaller size particles on 6 and 22 than on 14th. Furthermore, there appear to be more larger particles on 22nd than on 6th. The height of the two peaks in the size distribution on 14th is observed to increase whenever the AOT in 1030 nm exceeds that at 870 nm. In some cases a large peak around 1 μm is seen. Such a behavior in AOT may indicate the presence of mono-disperse aerosols in the atmosphere.

CONCLUSION

Data from an eight-channel sun-photometer operating in the 440–1030 nm range is analyzed to derive aerosol optical thickness, precipitable water

and aerosol size distribution for a location in Southern Russia during a field experiment held in July 1991. Data from a spectro-radiometer that measures direct-normal solar irradiance, diffuse and total hemi-spherical downward irradiance at the surface are also analyzed to yield AOT and a measure of the atmospheric transmission as a function of wavelength in about 70 channels from 300 to 580 nm. Comparison with FIFE'87 and FIFE'89 results show that although the correlation between AOT and PW is good similar to that in FIFE'87, the histogram of Ångström exponents show a mono-modal distribution similar to that in FIFE'89. The size distribution retrieved from the AOT versus wavelength curve using Twitty's method is consistent that derived from the solar aureole measurements using Nakajima's method. The time series of AOT clearly shows the effect of a cold front which moved through the area on July 12 bringing in clean, dry, Arctic air.

Acknowledgments

We are thankful to both Russian and American teams for our mutual collaborative work during the KUREX'91 campaign and after it. Students of the Moscow State University helped us with logistics. In addition, we would like to acknowledge discussions with Mr. Michael G. Khraponov from the Research Center "Planeta". Ms. Ruth Jones helped in the implementation of modified Twitty's algorithm onto the computer. Cimel sun-photometer data and analysis was made available by NASA's AERONET. We gratefully acknowledge funding from agencies in the former USSR and USA without which this work would never have been done. This work was supported in part by the Environmental Sciences Division of the U.S. Department of Energy as part of the Atmospheric Radiation Measurement Program under Contract No. DE-AC02-76CH00016.

References

Bruegge, C.J., Conel, J.E., Green, R.O., Margolis, J.S., Holm, R.G. and Toon, G. (1992) Water vapor column abundance retrievals during FIFE. *J. Geoph. Res.*, 97, D17: 18 759–18 768.

Dave, J.V. (1968) Subroutines for computing the parameter of the electromagnetic radiation scattered by a sphere. *I.B.M. Tech. Rept.* **320**: 3237.

Halthore, R.N., Bruegge, C.J. and Markham, B.L. (1990) Aerosol optical thickness measurements during FIFE'89. *Proc. AMS meeting*, pp. 121–125.

Halthore, R.N. and Markham, B.L. (1992) Boston, MA Overview of atmospheric correction and radiometric calibration efforts during FIFE. *J. Geoph. Res.*, 97, D17: 18 731–18 742.

Halthore, R.N., Markham, B.L. and Deering, D.W. (1992a) Atmospheric Correction and Calibration During KUREX-91. *Proc. IGARSS*, Houston, Tx. May. pp. 1278–1280.

Halthore, R.N., Markham, B.L., Ferrare, R.A. and Aro, T.O. (1992b) Aerosol Optical Properties over the mid-continental United States. *J. Geophys. Res.*, **97**, D17: 18 769–18 778.

Halthore, R.N., Eck, T.F., Holben, B.N. and Markham, B.L. (1997) Sun photometric measurements of atmospheric water vapor column abundance in the 940-nm band. *J. Geophys. Res.* **102**: 4343–4352.

Nakajima, T., Tanaka, M. and Yamauchi, T. (1983) Retrieval of the Optical Properties of Aerosols from Aureole and Extinction Data. *Appl. Optics*, **22**: 2951–2959.

Reagan, J.A., Pilewskie, P.A., Scott-Fleming, I.C., Herman, B.M. and Ben-David, A. (1987) "Extrapolation of Earth-Based Solar Irradiance Measurements to Exoatmospheric Levels for Broad-Band and Selected Absorption-Band Observations". *IEEE Trans. GeoScience Remote Sens.*, **GE-25**: 647–653.

Shaw, G.E. (1983) Sun Photometry. *Bull. Amer. Meteoro. Soc.*, **64**, 1: 4–10.

Twitty, J.T. (1974) The Inversion of Aureole Measurements to Derive Aerosol Size Distributions. *J. Atm. Sci.*, **32**, 584–591.

Vysotsky, A.V., Garadja, M.P., Nezval, E.L., Dorokhov, V.M., Klimova, T.N., Torgovitchev, V.A. and Khattatov, V.U. (1982) Development of an instrument for monitoring of the ultraviolet radiation. In "Monitoring of background pollution of natural media". Leningrad, Gidrometeoizdat, pp. 180–188.